Chemical Science

RSC Publishing

EDGE ARTICLE

View Article Online
View Journal | View Issue

Cite this: *Chem. Sci.*, 2013, **4**, 1345

Giant gemini surfactants based on polystyrene–hydrophilic polyhedral oligomeric silsesquioxane shape amphiphiles: sequential "click" chemistry and solution self-assembly†

Zhao Wang,[a] Yiwen Li,*[a] Xue-Hui Dong,[a] Xinfei Yu,[a] Kai Guo,[a] Hao Su,[a] Kan Yue,[a] Chys Wesdemiotis,[ab] Stephen Z. D. Cheng*[a] and Wen-Bin Zhang*[a]

This paper reports our recent investigations in the synthesis, characterization, and solution self-assembly of giant gemini surfactants consisting of two hydrophilic carboxylic acid-functionalized polyhedral oligomeric silsesquioxane (APOSS) heads and two hydrophobic polystyrene (PS) tails covalently linked *via* a rigid spacer (*p*-phenylene or biphenylene) (PS–$(APOSS)_2$–PS). The sequential "click" approach was employed in the synthesis, which involved thiol–ene mono-functionalization of vinyl-functionalized POSS, Cu(I)-catalyzed Huisgen [3 + 2] azide–alkyne cycloadditions for "grafting" polymer tails onto the POSS cages, and subsequent thiol–ene "click" surface functionalization. The study of their self-assembly in solution revealed a morphological transition from vesicles to wormlike cylinders and further to spheres as the degree of ionization of the carboxylic acid groups on POSS heads increases. It was found that the PS tails are generally less stretched in the micellar cores of these giant gemini surfactants than those of the corresponding single-tailed (APOSS–PS) giant surfactant. It was further observed that the PS tail conformations in the micelles were also affected by the length of the rigid spacers where the one with longer spacer exhibits even more stretched PS tail conformation. Both findings could be explained by the topological constraint imposed by the short rigid spacer in PS–$(APOSS)_2$–PS gemini surfactants. This constraint effectively increases the local charge density and leads to an anisotropic head shape that requires a proper re-distribution of the APOSS heads on the micellar surface to minimize the total electrostatic repulsive free energy. The study expands the scope of giant molecular shape amphiphiles and has general implications in the basic physical principles underlying their solution self-assembly behaviors.

Received 22nd October 2012
Accepted 11th January 2013

DOI: 10.1039/c3sc22297g

www.rsc.org/chemicalscience

Introduction

In the past decades, complex ordered structures based on the self-assembly of nano-building blocks have revolutionized many conventional technologies including electronics, data storage, and therapeutics.[1–5] To fabricate ordered structures across multiple length scales using the "bottom-up" approach, rigorous control and fine tuning of the nano-particle interactions are required.[6–9] Recently, a new class of amphiphiles named "shape amphiphiles" has emerged as hybrids of nano-building blocks that are incommensurate in terms of shapes and interactions. Owing to well-defined structure and precise modification, molecular nano-particles such as functionalized T8 polyhedral oligomeric silsesquioxane (POSS)[10–14] and [60]fullerene (C60),[15–17] have gained popularity as important building blocks for shape amphiphiles.

In analogy to "small-molecule surfactants", a unique type of shape amphiphile, called "giant surfactant" that possesses a nano-particle polar head tethered with a hydrophobic polymer tail,[18–21] has been designed and synthesized using both "grafting-from" and "grafting-onto" strategies.[22–26] As shown by both experimental data and computer simulation, not only could they self-assemble into diverse hierarchical supramolecular structures, but also distinct self-assembly behaviors could be observed based on tiny differences in the shape and symmetry of the nano-particle heads, as well as the geometry and topology of the tethered polymer tails.[15,27] For example, a giant surfactant consisting of carboxylic acid-functionalized POSS end-capped polystyrene (PS) (APOSS–PS) (Scheme 1a) has been synthesized by hydrosilylation and subsequent thiol–ene functionalization and found to self-organize into different micellar morphologies (spheres, cylinders, and vesicles) in selective solvents.[22] Unlike block copolymers,[28,29] the PS tails in the core of these micelles

[a]*Department of Polymer Science, College of Polymer Science and Polymer Engineering, The University of Akron, Akron, Ohio, 44325-3909, USA. E-mail: yl48@zips.uakron.edu; wz8@uakron.edu; scheng@uakron.edu*

[b]*Department of Chemistry, The University of Akron, Akron, Ohio, 44325-3601, USA*

† Electronic supplementary information (ESI) available: Details of characterization data including ^{1}H NMR, ^{13}C NMR spectra, FTIR spectra, and MALDI-TOF mass spectra of the products, as well as DLS results. See DOI: 10.1039/c3sc22297g

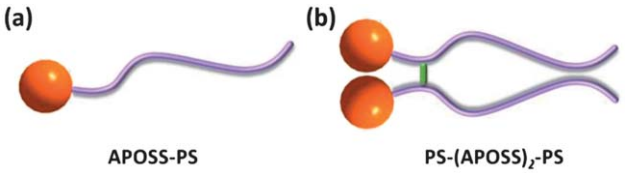

Scheme 1 Cartoon illustration of (a) giant surfactant and (b) giant gemini surfactant.

were found to be highly stretched, a feature reminiscent of small-molecule surfactants.[22,30] Based on the similar concept, another class of shape amphiphiles, so-called "giant lipid", which consists of two polymer tails of symmetric/asymmetric compositions tethered to one nano-particle head, has also been designed and synthesized.[24,26] It remains a wide open field to explore other variations of shape amphiphiles in analogy to their small-molecule counterparts.

Gemini surfactants are composed of two conventional single-chained surfactant molecules covalently linked by a spacer located at, or close to the head groups.[31,32] Compared with single-chained surfactants, gemini surfactants often display distinct physical properties, such as enhanced surface activity and intriguing assembled morphologies at interfacial regions in solution.[33–38] Specifically, the critical micellization concentrations (cmc) of gemini surfactants usually are much lower than those of the corresponding conventional surfactants when the tail length is comparably short.[39] Recent studies have also shown that the chemical and physical natures of the spacer (length, rigidity, chemical composition) play a significant role in the self-assembly of gemini surfactants in aqueous solution.[40,41] Our question is whether such differences also exist in POSS-based "giant gemini surfactants" (Scheme 1b). A model giant gemini surfactant could be constructed by covalently linking APOSS–PS *via* a rigid spacer near the head groups (Scheme 2). The overall shape of giant gemini surfactant is anisotropic and thus, possesses symmetry breaking. A comparison between the self-assembly of APOSS–PS and the dimer shall shed light into the impact of topological constraints on the self-assembly of shape amphiphiles in general.

In this article, we report our efforts in the synthesis, characterization and solution self-assembly behaviours of a new class of POSS-based shape amphiphiles – the "giant gemini surfactants", PS–$(APOSS)_2$–PS. They can be synthesized by a sequential "click" approach with precisely controlled molecular weight, spacer, and surface groups on POSS (Scheme 2). The micellar morphologies of PS–$(APOSS)_2$–PS in solution were studied and compared to that of APOSS–PS under similar conditions. The results revealed several differences in the conformation of hydrophobic polymer tails in the micelle core. A possible explanation was also attempted.

Results and discussion

Sequential "click" synthesis

Vinyl-functionalized POSS (VPOSS) has been recognized as a versatile building block for constructing POSS-based shape amphiphiles owing to its high compatibility with various polymerization methods and the ease of subsequent transformation of vinyl groups into various functionalities by thiol–ene click reactions.[22–24,26] A variety of dual functional VPOSS derivatives have been developed to synthesize a library of "giant surfactants" over the past few years.[22,23,25,26] We recently demonstrated a novel triple functional VPOSS derivative, HO–(VPOSS)–OH, for the preparation of "giant lipids" possessing two symmetric/asymmetric polymer tails.[26] Herein, we show that HO–(VPOSS)–OH can be easily adapted to synthesize "giant gemini surfactants" using the sequential "click" approach.[25] Two homologous giant gemini surfactants, denoted as series **1** and **2**, were designed to possess phenyl and biphenyl groups as the spacer, respectively.

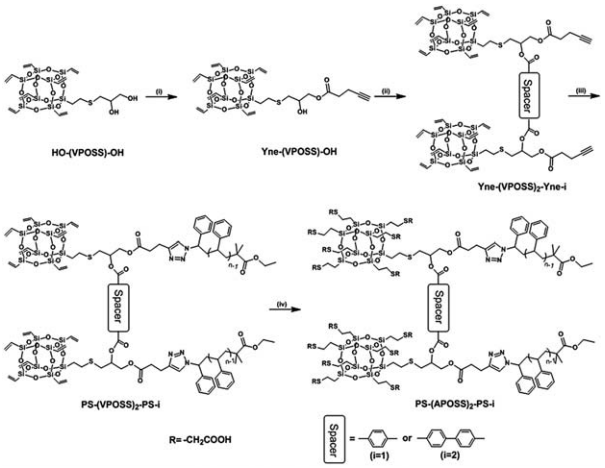

Scheme 2 Synthetic route towards giant gemini surfactants : (i) 4-pentynoic acid, DPTS, DIPC, dry CH_2Cl_2, 0 °C, 50%; (ii) terephthalic acid or biphenyl-4,4′-dicarboxylic acid, DPTS, DIPC, dry DMF, 0 °C, 32% for Yne–$(VPOSS)_2$–Yne-1, and 39% for Yne–$(VPOSS)_2$–Yne-2; (iii) PS–N_3, CuBr, PMDETA, toluene, 25 °C, 91% for PS–$(VPOSS)_2$–PS-1, and 88% for PS–$(VPOSS)_2$–PS-2; (iv) 2-mercaptoacetic acid, DMPA, THF, 25 °C, 15 min, 79% for PS–$(APOSS)_2$–PS-1, and 83% for PS–$(APOSS)_2$–PS-2.

The "clickable" dimeric VPOSS derivatives were synthesized by stoichiometry-controlled, selective esterification of the primary hydroxyls on HO–(VPOSS)–OH with 4-pentynoic acid to give Yne–(VPOSS)–OH followed by dimerization with a rigid di-acid spacer to give Yne–$(VPOSS)_2$–Yne (Scheme 2). As indicated by the ^{1}H NMR spectrum of the crude product (data not shown), the esterification preferably occurred on the primary hydroxyl of HO–(VPOSS)–OH with <10% isomer detected, due to less steric hindrance and higher reactivity. The slightly different polarity of final products allows chromatographic separation of the two isomers. The desired Yne–(VPOSS)–OH was finally isolated in a good yield (50%) and fully characterized by ^{1}H NMR spectrometry (Fig. S1†) and other techniques. In the ^{1}H NMR spectrum, the characteristic resonances at δ (4.27–4.14) and 3.94 ppm with an integration ratio of 2 : 1 correspond to the methylene protons (b) near the ester bond and methane protons (c) near to hydroxyl group, respectively. No resonance appeared at δ 5.03 and 3.77 ppm that can be attributed to the isomer, confirming the well-defined structure and high purity. Furthermore, the observed *m*/*z* value (842.34 Da) in the MALDI-TOF spectrum agreed perfectly with the calculated value ($C_{24}H_{36}NaO_{15}SSi_8$ 842.98 Da). Two "clickable" VPOSS dimers

were then successfully synthesized with phenylene (Yne–(VPOSS)$_2$–Yne-1) or bi-phenylene groups (Yne–(VPOSS)$_2$–Yne-2) as spacers by esterification with the corresponding di-acids in DMF. Both products were thoroughly characterized by ^{1}H NMR, ^{13}C NMR, FT-IR, and MALDI-TOF mass spectrometry to establish their identity and the uniformity of the molecular structures. For example, the resonance at δ (4.27–4.14) and 3.94 ppm assigned to the protons between the ester bond and the hydroxyl group completely shifted to new positions at δ 5.39, 4.55, and 4.43 ppm, suggesting complete reaction (Fig. 1a). The occurrence of new resonance in the aromatic region (δ 8.09 ppm) corresponded to those on the phenylene ring bridging the two VPOSS cages. In the MALDI-TOF mass spectrum (Fig. S2a†), only one strong peak matching the proposed structures of the targeted molecules was observed. The observed peak at m/z 1793.13 agreed well with the calculated monoisotopic molecular mass for Yne–(VPOSS)$_2$–Yne-1 ($C_{56}H_{74}NaO_{32}S_2Si_{16}$, 1792.98 Da). The characterizations of Yne–(VPOSS)$_2$–Yne-2 were similar and can be found in the ESI (Fig. S2b and S3†). All evidence supports the successful synthesis of "clickable" VPOSS dimeric precursors.

The recently reported sequential "click" approach[25] was then employed to prepare the POSS-based "giant gemini surfactants" (PS–(APOSS)$_2$–PS) (Scheme 2). The first CuAAC "click" reaction between azido-functionalized PS chains (PS–N$_3$, M_n = 3.2 kg mol^{-1}, PDI = 1.05) and Yne–(VPOSS)$_2$–Yne under typical conditions successfully afforded the precursor PS–(VPOSS)$_2$–PS in a good yield of ~90%. For PS–(VPOSS)$_2$–PS-1, the disappearance of the strong characteristic vibrational band for the azide group at ~2094 cm^{-1} and the appearance of the vibrational band at ~1087 cm^{-1} (Si–O–Si on POSS) in the FTIR spectrum (Fig. S4†) suggested the complete consumption of the PS–N$_3$ and successful incorporation of POSS. The intact VPOSS cages were also confirmed by the resonance signals at δ (6.14–5.84) ppm in the ^{1}H NMR spectrum (Fig. 1b), with an integration ratio of about 21/2 when compared to the chain end methylene protons (h) at δ (3.60–3.36) ppm. The SEC diagram of PS–(VPOSS)$_2$–PS-1 (Fig. 2) shows a mono-modal symmetric peak at much lower retention volume than that of PS–N$_3$, which is consistent with the increased molecular weight. Furthermore, in the MALDI-TOF mass spectrum (Fig. 3a), a single narrow molecular weight distribution can be clearly observed under the linear modal despite the relatively high molecular weight of PS–(VPOSS)$_2$–PS-1. Although mono-isotopic resolution is not possible in this molecular weight range,[42] the average molecular weights of the peaks match well with the calculated values (*e.g.*, for 52-mer with the formula of $C_{484}H_{512}N_6NaO_{36}S_2Si_{16}$, observed m/z 7526.71 Da *vs.* calcd. 7525.75 Da). Similar characterizations were also performed for PS–(VPOSS)$_2$–PS-2 (see Fig. S5a† for NMR, Fig. S6† for SEC, and Fig. 3b for MALDI-TOF mass spectrum). All the data attest to the homogeneity and purity of the samples.

Thiol–ene "click" chemistry has been demonstrated as an efficient, robust and modular tool for "simultaneous, multiple-site functionalization" in the construction of POSS-based shape amphiphiles.[43–45] Diverse functional groups have been introduced onto the POSS periphery, including hydrophilic,[14,22,23,25,26] fluorophilic functionalities[14,24,46] and bioactive moieties.[23,47] The second "click" reaction thus involves the thiol–ene modification of the VPOSS periphery to introduce chemical amphiphilicity. A commercially available thiol, 2-mercaptoacetic acid was used. After the reaction, PS–(VPOSS)$_2$–PS was converted completely to PS–(APOSS)$_2$–PS, as revealed by the disappearance of vinyl protons in the resonance range of δ (6.14–5.84) ppm in the ^{1}H NMR spectrum (Fig. 1c) and sp2 carbon signals at δ 137.15 and 128.67 ppm in the ^{13}C NMR spectrum (Fig. S7†) of PS–(APOSS)$_2$–PS-1. The new characteristic resonance emerging in the range of δ 2.89–2.60 ppm in the ^{1}H NMR spectrum can be attributed to the formation of thiol ether bonds (protons

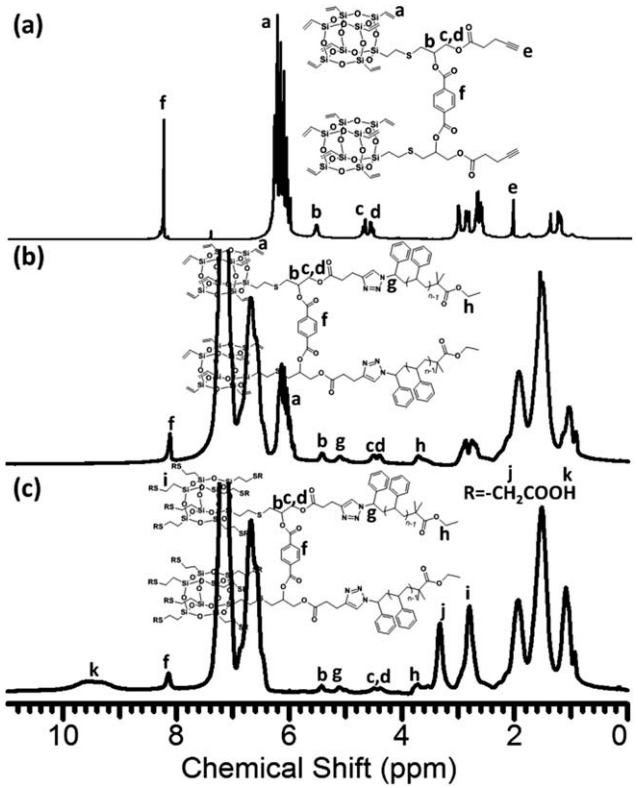

Fig. 1 ^{1}H NMR spectra of (a) Yne–(VPOSS)$_2$–Yne-1, (b) PS–(VPOSS)$_2$–PS-1, and (c) PS–(APOSS)$_2$–PS-1.

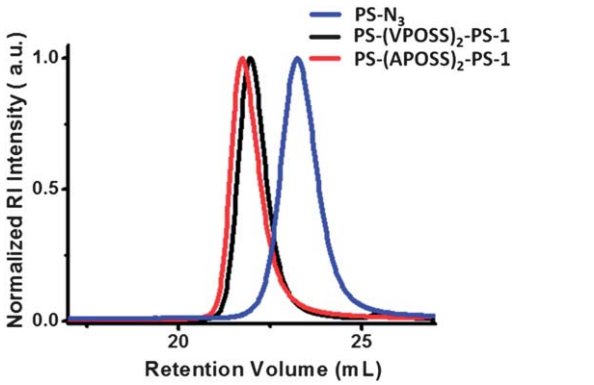

Fig. 2 SEC overlay of PS–N$_3$ (blue curve), PS–(VPOSS)$_2$–PS-1 (black curve) and PS–(APOSS)$_2$–PS-1 (red curve).

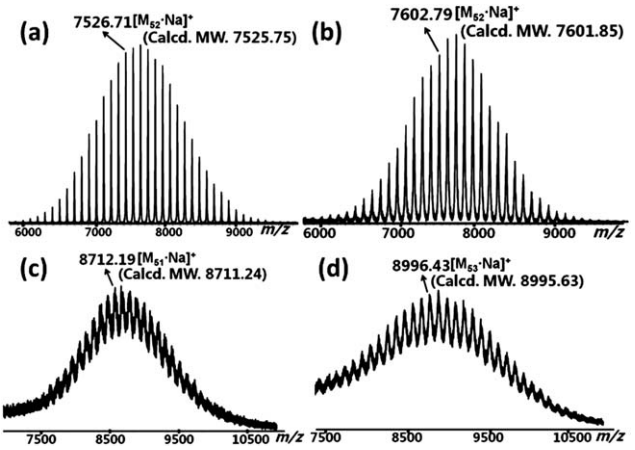

Fig. 3 MALDI-TOF mass spectra of (a) PS–$(VPOSS)_2$–PS-1, (b) PS–$(VPOSS)_2$–PS-2, (c) PS–$(APOSS)_2$–PS-1, and (d) PS–$(APOSS)_2$–PS-2.

(i) in Fig. 1c). Compared with PS–$(VPOSS)_2$–PS-1, a broad characteristic peak appears in the range of δ (10.05–9.00) ppm (protons (k) in Fig. 1c) in the ^{1}H NMR spectrum and a strong absorbance band at around 3200 cm^{-1} emerges in the FTIR spectrum (Fig. S4†). Both of the results provide direct evidence for the carboxylic acid hydrogen bonding formation. Moreover, the SEC diagram of PS–$(APOSS)_2$–PS-1 (Fig. 2) exhibits a single symmetric peak but shifting to a slightly lower retention volume relative to that of PS–$(VPOSS)_2$–PS-1 due to a small increase in molecular weight. In addition, the structural homogeneity and purity of the targeted product are also validated by MALDI-TOF mass spectrometry (Fig. 3c). The overview of the spectrum obtained in the linear mode exhibits one single narrow distribution with molecular weights in accordance with the proposed structure. Furthermore, it is also clear that PS–$(VPOSS)_2$–PS-1 displays two resonances at δ −66.0 ppm ($-SiCH_2CH_2S-$) and −75.1 ppm ($-SiCH{=}CH_2$) while PS–$(APOSS)_2$–PS-1 exhibits a single resonance at δ −66.0 ppm in the ^{29}Si NMR spectra (Fig. S8†), indicating the successful thiol–ene multiple addition reaction. Again, PS–$(APOSS)_2$–PS-2 was also successfully confirmed by ^{1}H NMR (Fig. S5b†), ^{13}C NMR (Fig. S9†), SEC (Fig. S6†) and MALDI-TOF mass spectrometry (Fig. 3d). Therefore, it can be concluded that the POSS-based giant gemini surfactants have been readily synthesized by the sequential "click" approach and possess precisely-defined structures as designed.

Solution self-assembly

Generally speaking, the formation of thermodynamically stable micelles of diverse morphologies in diblock copolymers is driven by three factors: the stretching of the micelle core-forming blocks, the interfacial tension between the micelle core and solvent outside, and the repulsive interactions among corona-forming blocks.[48–50] The micellar morphologies are thus dominated by molecular and solution parameters that affect each of the three contributions,[51,52] including chemical composition of polymers, overall molecular weight, macromolecular architecture, nature of common solvent, water content in solution, polymer concentration, pH value, temperature, and presence of additives, *etc.* In the system of APOSS–PS conjugates, it was evident that the free energy from interactions among corona-forming chains does not exist while the interactions among APOSS heads greatly contribute to the overall free energy.[22] In this case, it was found that the free energy from these repulsive interactions becomes the dominating term in the total free energy of the system.[22]

In the current study, we employed a similar method as we reported before[22] with low NaOH concentration to prepare the thermodynamically stable micelles with different morphologies for further investigation. Deionized water was slowly added at a rate of 10 μL h^{-1} into a vial containing 2 g of a stock solution of PS–$(APOSS)_2$–PS in a common solvent (1,4-dioxane or DMF) with an initial concentration of 2.8 wt%. The micelle formation occurred at a water content of about 23% in 1,4-dioxane and about 27% in DMF solution for both samples, respectively. More water was continuously added until a final water content of 70 wt%. Although the micellar morphology changed with the increase of the water content, we purposely chose to compare the thermodynamically stable micellar morphologies at identical water content (>70 wt%) to investigate the effect of different common solvents on the ionization of the multiple carboxylic acid groups and the resulting morphologies. The measurement of micelle solution parameters (FT-IR spectra of freeze-dried samples from micelle solution) was performed at this time before dialysis to reveal environmental characteristics of the micelles. Stable micelles were obtained by dialyzing the micelle solutions against deionized water for 3 days to remove the organic solvent.

The self-assembled micellar morphologies were investigated utilizing TEM and DLS techniques. Fig. 4 includes two sets of bright field TEM images of micelles formed in different common solvents for both PS–$(APOSS)_2$–PS-1 and PS–$(APOSS)_2$–PS-2, respectively. The high glass transition temperature of PS tails "froze" the micellar morphology at the state that it was formed, so the cryo-TEM technique was not necessary.[22] The self-assembled structures of PS–$(APOSS)_2$–PS-1 (with phenylene group as the spacer) in solution are discussed here and PS–$(APOSS)_2$–PS-2 exhibited similar morphologies. Different common solvents were used to control the degree of ionization of the carboxylic acid groups on the POSS cages, which changed the interactions among the APOSS heads and thus the morphology. From the TEM images, the radius of the hydrophobic PS core (R_i) could be measured. In Fig. 4a, bi-layered vesicles formed in 1,4-dioxane–water mixture solution could be clearly observed with an average wall thickness of (10.4 ± 0.4) nm. Assuming a diameter of 1.0 nm for the APOSS cage,[22] the radius of the PS core of the vesicles (R_1) could be estimated to be (4.2 ± 0.2) nm. In addition, DLS measurement also revealed a hydrodynamic radius (R_h) of ~60 nm with a narrow size distribution for the vesicles (Fig. S10a†). In DMF–water mixed solution, the worm-like cylindrical micelles were formed as shown by bright field TEM images in Fig. 4b. It was found that the average diameter of these cylindrical micelles is ~(11.4 ± 0.6) nm, suggesting a PS core radius (R_2) of ~(4.7 ±

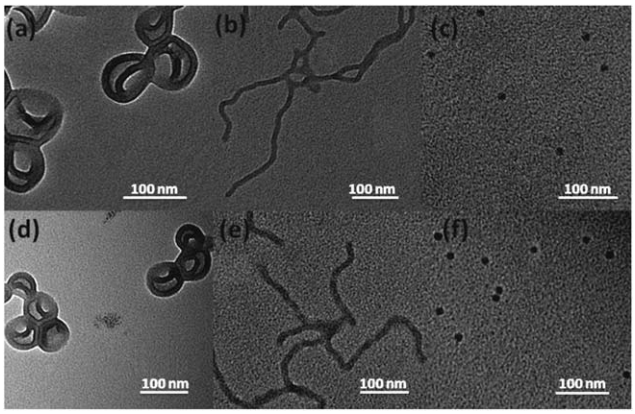

Fig. 4 TEM images of (a–c) PS–$(APOSS)_2$–PS-1 and (d–f) PS–$(APOSS)_2$–PS-2 micelles in solution with an initial concentration of 2.8% and a final water content of >70 wt% using the following common solvents: (a and d) 1,4-dioxane, (b and e) DMF, and (c and f) DMF/NaOH.

0.3) nm. The spherical micelles were formed when a mixture of DMF and 0.05 M NaOH with molar ratio ($N_{NaOH}/N_{COOH} = 0.07$) was used as the common solvent. In Fig. 4c, the average diameter of the spheres was observed to be (13.9 ± 0.7) nm, which was also supported by DLS experiments (Fig. S10b†). Thus, the hydrophobic PS core radius (R_3) is (6.0 ± 0.3) nm. The micelle formation of PS–$(APOSS)_2$–PS-2 was performed under the identical conditions. Based on the bright field TEM images in Fig. 4d–f, R_i could be similarly calculated for different micellar morphologies. From the R_i values, the average surface area per two chains (A_i) of one giant gemini surfactant molecule could be quantitatively estimated using the correction eqn (1) as follows:[22,46]

$$A_i = \frac{2iV_sN_{PS}}{fR_i} \quad (1)$$

where i is the micellar geometry dependent factor ($i = 3$ for sphere, $i = 2$ for cylinder and $i = 1$ for vesicle), V_s is the volume per PS monomer (0.167 nm^3), N_{PS} is the degree of polymerization, and f is the volume fraction of PS tails in the micellar core. By definition, f approaches unity if PS tails were sufficiently dense in the cores when the water content is high enough in the environment. On the other hand, the A_i values for APOSS–PS are considered as the average surface area per two chains and thus, per two molecules. For comparison, the data from ref. 22 were adapted. All the results are summarized in Table 1.

While the above observations for giant gemini surfactants PS–$(APOSS)_2$–PS are qualitatively similar to that of the "giant surfactant" APOSS–PS as reported previously,[22] we are particularly interested in the morphological transformation mechanism and tail conformation inside the micellar core. It turns out that the micellar morphological transformation of PS–$(APOSS)_2$–PS is driven by essentially the same mechanism to that of APOSS–PS.[22] While corona interaction does not exist in both systems, the interactions among the APOSS heads play the key role in determining the morphological transformation. With increasing the degree of ionization by changing common solvents, the repulsive force among the APOSS heads is enhanced. The giant gemini surfactant molecules need to spontaneously increase the A_i in order to minimize the electrostatic free energy of the APOSS heads, which results in the micellar morphological transitions from vesicles to wormlike cylinders and further to spheres.[22,46,53,54] By using FT-IR spectrometry, the degrees of ionization (α) of carboxylic acid groups on POSS cages were directly calculated to be 29% (for vesicle), 35% (for cylinder), and 38% (for sphere), respectively (see SI and Fig. S12†). The results are in qualitative agreement with previous studies.[22] All the results are in good accordance with the increase of A_i in the order of $A_{vesicle} < A_{cylinder} < A_{sphere}$ respectively, affirming the proposed transformation mechanism.

A direct result of increasing A_i is the stretching of PS chains in the micellar core so as to compensate the increased surface area and surface free energy per chain by decreasing the aggregation number and the total surface area of the micelle.[46] The highly stretched polymer chain in the micellar core is a unique feature of giant surfactants in comparison to block copolymers.[15,22] To quantify the degree of stretching, the stretching ratio (S) can be calculated as a ratio of the PS tail dimension in different micellar cores (R_i) to its average unperturbed chain dimension (R_0) as shown in eqn (2):

$$S = \frac{R_i}{R_0} = \frac{R_i}{b}\left(\frac{6.92}{N_{PS}}\right)^{\frac{1}{2}} \quad (2)$$

where b is the Kuhn length ($b = 1.8$ nm) for PS.[15] The results are listed in Table 1. It is evident that the PS tails are less stretched in the micellar cores of PS–$(APOSS)_2$–PS micelles than those in APOSS–PS micelles. Although the polymer tail conformation in the micelles is length-dependent,[15] a comparison between the stretching ratios of PS tails in the micellar cores of PS–$(APOSS)_2$–PS and those in the cores of the APOSS–PS micelles is still meaningful because of their very similar PS tail lengths (3.2k *vs.* 2.8k). It suggests that the generally less stretched conformation in PS–$(APOSS)_2$–PS is an effect of architecture rather than an effect of molecular weight. More intriguingly, the PS tails in the cores of PS–$(APOSS)_2$–PS micelles are found to be less stretched in the system with a short spacer (phenylene) than that with a long spacer (biphenylene), which is somewhat counter-intuitive. Nevertheless, both observations could be explained by the anisotropic head shape of giant gemini surfactants as a result of the topological constraint imposed by the short rigid spacers near the heads.

In the PS–$(APOSS)_2$–PS system, the A_i values are determined not only by the mean thermodynamic distance between neighboring gemini molecules (d_T), but also by the length of the rigid spacer (d_s). The rigid spacer length is considered to be fixed and can be estimated by the Accelrys Cerius^2 package using the universal force field.[14] As a first approximation, qualitatively assuming A_i represents the area of a rectangle shape due to anisotropy, and a simple model was established to understand the importance of anisotropy (see in Fig. 5). From the model, the A_i has the following relationship to d_T and d_s (eqn (3)):

$$A_i = (d_s + d_T)d_T \quad (3)$$

Table 1 Morphologies and physical parameters of PS–APOSS and PS–$(APOSS)_2$–PS micelles formed using different common solvents

Sample	Micelle[a]	Common solvent	R_i (nm)[b]	$M_{n,PS}$[c] (g mol^{-1})	S[d]	A_i[e] (nm^2)	d_s[f] (nm)	d_T (nm)[g]
APOSS–PS	V	1,4-Dioxane	4.5 ± 0.2	2.8k	1.27 ± 0.06	2.08 ± 0.08	—	1.02 ± 0.02
APOSS–PS	C	DMF	6.0 ± 0.3	2.8k	1.69 ± 0.09	3.12 ± 0.16	—	1.25 ± 0.04
APOSS–PS	S	DMF/NaOH	6.3 ± 0.3	2.8k	1.77 ± 0.08	4.46 ± 0.22	—	1.49 ± 0.06
PS–$(APOSS)_2$–PS-1	V	1,4-Dioxane	4.2 ± 0.2	3.2k	1.11 ± 0.05	2.55 ± 0.12	0.58	1.33 ± 0.03
PS–$(APOSS)_2$–PS-1	C	DMF	4.7 ± 0.3	3.2k	1.24 ± 0.08	4.55 ± 0.30	0.58	1.86 ± 0.13
PS–$(APOSS)_2$–PS-1	S	DMF/NaOH	6.0 ± 0.3	3.2k	1.58 ± 0.10	5.35 ± 0.27	0.58	2.04 ± 0.12
PS–$(APOSS)_2$–PS-2	V	1,4-Dioxane	4.6 ± 0.2	3.2k	1.21 ± 0.05	2.33 ± 0.10	0.97	1.12 ± 0.04
PS–$(APOSS)_2$–PS-2	C	DMF	5.6 ± 0.3	3.2k	1.48 ± 0.08	3.82 ± 0.21	0.97	1.53 ± 0.08
PS–$(APOSS)_2$–PS-2	S	DMF/NaOH	6.6 ± 0.3	3.2k	1.74 ± 0.08	4.87 ± 0.23	0.97	1.77 ± 0.09

[a] Morphologies observed in TEM (S: sphere C: cylinder; V: vesicle). [b] R_i is the radius of the hydrophobic PS core measured based on the TEM images. [c] Molecular weight of each single PS tail from SEC and ^{1}H NMR measurements. [d] S is the stretching ratio calculated based on the ratio of R_i and unperturbed chain dimension R_0. [e] A_i is the average surface area per two PS chains. [f] d_s is the rigid spacer length, which could be obtain from the Accelrys Cerius^2 package using the universal force field. [g] d_T is the mean thermodynamic distance between neighboring gemini molecules. The data for PS–APOSS were derived from ref. 22.

Therefore, d_T can be derived from A_i and d_s as in eqn (4):

$$d_T = \sqrt{A_i + \frac{d_s^2}{4}} - \frac{d_s}{2} \quad (4)$$

The calculated d_T values are summarized in Table 1. Note that this equation should work precisely for systems with little curvature system such as in the vesicle bilayers, but may only represent a crude approximation in micelles with larger curvatures such as spheres and cylinders. However, the results should serve well for the purpose of a semi-quantitative comparison between different samples of the same micelle type with similar sizes. An additional note is that the above-mentioned model assumes $d_s < d_T$ for an effective topological constraint between two heads in the same gemini surfactant. This is true in the two samples under study (Table 1). However, in the case of $d_s \geq d_T$, the physical picture might be quite different.[39] Similarly, we could also calculate the d_T values in different APOSS–PS micelles by assuming A_i represents the area of two square shapes (Fig. S13†), which are also listed in Table 1.

The first observation in this model is that the rigid short spacer effectively brings the two APOSS heads closer to each other, leading to an increased local charge density. It may well attract more counter-ions around the head groups than that in the single-chained giant surfactant APOSS–PS. The intermolecular distances (d_T) shall thus increase to reduce the actual electrostatic repulsive energy. For the same type of micellar morphology, a larger d_T would mean more inter-molecular space for the chain to relax and thus a less stretched chain conformation. This accounts for the fact that PS–$(APOSS)_2$–PS generally exhibits less stretched polymer chain conformation for samples with the same type of micellar morphology. The effect of the rigid spacer is now also evident. This analysis agrees with the prediction from computer simulations of small molecular gemini surfactants.[39] All of the current established models for gemini surfactants could only explain the qualitative difference between PS–$(APOSS)_2$–PS gemini surfactants and corresponding APOSS–PS surfactants. A quantitative discussion on spacer length effects is very difficult.[39] We could only predict that, for the same type of micellar morphology, the shorter the spacer of giant gemini surfactant is, the more effectively it increases the local charge density and the intermolecular distance d_T, and the less stretched the polymer tails in the micellar core become. It is anticipated that a systematic variation of the length and rigidity of the spacer of giant gemini surfactants shall allow further tailoring of the physical and chemical properties as well as self-assembly behaviors of this novel class of materials.

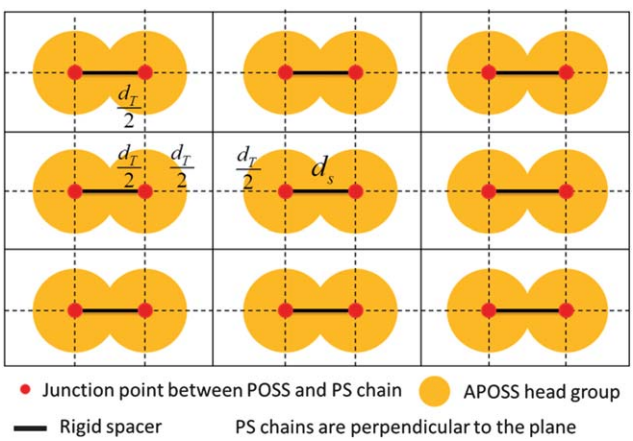

Fig. 5 Proposed model of giant gemini surfactants packing on the micelle surface.

Conclusions

In summary, a new class of shape amphiphiles called "giant gemini surfactants" consisting of two hydrophilic POSS heads and two hydrophobic PS tails covalently attached through rigid spacers has been successfully prepared and their self-assembly behaviors in solution were studied. The sequential "click" approach was employed in the synthesis, which involved thiol–ene mono-functionalization of vinyl-functionalized POSS, Cu(I)-catalyzed Huisgen [3 + 2] azide–alkyne cycloadditions for "grafting" polymer tails onto the POSS cages, and subsequent thiol–ene "click" surface functionalization. The study of their

self-assembly in solution revealed a morphological transition from vesicles to wormlike cylinders and further to spheres as the degree of ionization of the carboxylic acid groups on POSS heads increases. It was found that the PS tails in the micellar cores of these giant gemini surfactants are generally less stretched than those of the corresponding single-chained giant surfactant. It was further observed that the PS tail conformations in the micelles were also affected by the length of the rigid spacers where the one with longer spacer actually exhibits even more stretched PS chain conformation. Both findings could be explained by the topological constraint imposed by the short rigid spacer in gemini surfactants which effectively increases the local charge density by bringing heads closer to each other and leads to an anisotropic overall head shape that requires a proper re-distribution on the micellar surface to minimize the total electrostatic repulsive free energy of micelles. The study expands the scope of giant molecular shape amphiphiles and has general implications in the basic physical principles underlying their solution self-assembly behaviors. In addition, a systematic study of the spacer effects in the self-assembly of giant gemini surfactants and hierarchical structure formation in solution, bulk, and thin-films is an intriguing ongoing project in our laboratory and will be discussed in future publications.

Acknowledgements

This work was supported by the National Science Foundation (DMR-0906898) and the Joint-Hope Education Foundation.

Notes and references

1 M.-C. Daniel and D. Astruc, *Chem. Rev.*, 2004, **104**, 293.
2 J. C. Love, L. A. Estroff, J. K. Kriebel, R. G. Nuzzo and G. M. Whitesides, *Chem. Rev.*, 2005, **105**, 1103.
3 J. D. Hartgerink, E. Beniash and S. I. Stupp, *Science*, 2001, **294**, 1684.
4 M. Reches and E. Gazit, *Science*, 2003, **300**, 625.
5 S. C. Glotzer and M. Engel, *Nature*, 2011, **471**, 309.
6 G. M. Whitesides and B. Grzybowski, *Science*, 2002, **295**, 2418.
7 S. C. Glotzer and M. J. Solomon, *Nat. Mater.*, 2007, **6**, 557.
8 P. F. Damasceno, M. Engel and S. C. Glotzer, *Science*, 2012, **337**, 453.
9 H. Xiong, D. Van Der Lelie and O. Gang, *J. Am. Chem. Soc.*, 2008, **130**, 2442.
10 K. Tanaka and Y. Chujo, *J. Mater. Chem.*, 2012, **22**, 1733.
11 S.-W. Kuo and F.-C. Chang, *Prog. Polym. Sci.*, 2011, **36**, 1649.
12 M. F. Roll, M. Z. Asuncion, J. Kampf and R. M. Laine, *ACS Nano*, 2008, **2**, 320.
13 D. B. Cordes, P. D. Lickiss and F. Rataboul, *Chem. Rev.*, 2010, **110**, 2081.
14 Y. Li, W.-B. Zhang, I.-F. Hsieh, G. Zhang, Y. Cao, X. Li, C. Wesdemiotis, B. Lotz, H. Xiong and S. Z. D. Cheng, *J. Am. Chem. Soc.*, 2011, **132**, 10712.
15 X. Yu, W.-B. Zhang, K. Yue, X. Li, H. Liu, Y. Xin, C.-L. Wang, C. Wesdemiotis and S. Z. D. Cheng, *J. Am. Chem. Soc.*, 2012, **134**, 7780.
16 W.-B. Zhang, Y. Tu, R. Ranjan, R. M. Van Horn, S. Leng, J. Wang, M. J. Polce, C. Wesdemiotis, R. P. Quirk, G. R. Newkome and S. Z. D. Cheng, *Macromolecules*, 2008, **41**, 515.
17 X.-H. Dong, W.-B. Zhang, Y. Li, M. Huang, S. Zhang, R. P. Quirk and S. Z. D. Cheng, *Polym. Chem.*, 2012, **3**, 124.
18 Z. Zhang, M. A. Horsch, M. H. Lamm and S. C. Glotzer, *Nano Lett.*, 2003, **3**, 1341.
19 K. Velonia, A. E. Rowan and R. J. M. Nolte, *J. Am. Chem. Soc.*, 2002, **124**, 4224.
20 I. C. Reynhout, J. J. L. M. Cornelissen and R. J. M. Nolte, *Acc. Chem. Res.*, 2009, **42**, 681.
21 J. C. M. Van Hest, D. A. P. Delnoye, M. W. P. L. Baars, M. H. P. Van Genderen and E. W. Meijer, *Science*, 1995, **268**, 1592.
22 X. Yu, S. Zhong, X. Li, Y. Tu, S. Yang, R. M. Van Horn, C. Ni, D. J. Pochan, R. P. Quirk, C. Wesdemiotis, W.-B. Zhang and S. Z. D. Cheng, *J. Am. Chem. Soc.*, 2010, **132**, 16741.
23 W.-B. Zhang, Y. Li, X. Li, X. Dong, X. Yu, C.-L. Wang, C. Wesdemiotis, R. P. Quirk and S. Z. D. Cheng, *Macromolecules*, 2011, **44**, 2589.
24 J. He, K. Yue, Y. Liu, X. Yu, P. Ni, K. A. Cavicchi, R. P. Quirk, E.-Q. Chen, S. Z. D. Cheng and W.-B. Zhang, *Polym. Chem.*, 2012, **3**, 2112.
25 K. Yue, C. Liu, K. Guo, X. Yu, M. Huang, Y. Li, C. Wesdemiotis, S. Z. D. Cheng and W.-B. Zhang, *Macromolecules*, 2012, **45**, 8126.
26 Y. Li, X.-H. Dong, K. Guo, Z. Wang, Z. Chen, C. Wesdemiotis, R. P. Quirk, W.-B. Zhang and S. Z. D. Cheng, *ACS Macro Lett.*, 2012, **1**, 834.
27 M. A. Horsch, Z. Zhang and S. C. Glotzer, *Phys. Rev. Lett.*, 2005, **95**, 056105.
28 Y. Yu and A. Eisenberg, *J. Am. Chem. Soc.*, 1997, **119**, 8383.
29 Y. Yu, L. Zhang and A. Eisenberg, *Macromolecules*, 1998, **31**, 1144.
30 K. Holmberg, B. Jönsson, B. Kronberg and B. Lindman, *Surfactants and Polymers in Aqueous Solution*, Wiley, Chichester, U.K., 2003.
31 F. M. Menger and J. S. Keiper, *Angew. Chem., Int. Ed.*, 2000, **39**, 1906.
32 F. M. Menger and C. A. Littau, *J. Am. Chem. Soc.*, 1993, **115**, 10083.
33 S. Karaborni, K. Esselink, P. A. J. Hilbers, B. Smit, J. Karthäuser, N. M. Van Os and R. Zana, *Science*, 1994, **266**, 254.
34 R. Zana, *Langmuir*, 1996, **12**, 1208.
35 S. Manne, T. E. Schäffet, Q. Huo, P. K. Hansma, D. E. Morse, G. D. Stucky and I. A. Aksayt, *Langmuir*, 1997, **13**, 6382.
36 M. Zhou, P. R. Nemade, X. Lu, X. Zeng, E. S. Hatakeyama, R. D. Noble and D. L. Gin, *J. Am. Chem. Soc.*, 2007, **129**, 9574.
37 G. P. Sorenson, K. L. Coppage and M. K. Mahanthappa, *J. Am. Chem. Soc.*, 2011, **133**, 14928.
38 J. Mondal, M. Mahanthappa and A. Yethiraj, *J. Phys. Chem. B*, 2012, DOI: 10.1021/jp304933k.

39 T. A. Camesano and R. Nagarajan, *Colloids Surf., A*, 2000, **167**, 165.
40 R. Zana, *J. Colloid Interface Sci.*, 2002, **248**, 203.
41 F. M. Menger and B. N. A. Mbadugha, *J. Am. Chem. Soc.*, 2001, **123**, 875.
42 Y. Li, W.-B. Zhang, J. E. Janoski, X. Li, X. Dong, C. Wesdemiotis, R. P. Quirk and S. Z. D. Cheng, *Macromolecules*, 2011, **44**, 3328.
43 A. B. Lowe, *Polym. Chem.*, 2010, **1**, 17.
44 C. E. Hoyle and C. N. Bowman, *Angew. Chem., Int. Ed.*, 2010, **49**, 1540.
45 M. J. Kade, D. J. Burke and C. J. Hawker, *J. Polym. Sci., Part A: Polym. Chem.*, 2010, **48**, 743.
46 J. Xu, X. Li, C. M. Cho, C. L. Toh, L. Shen, K. Y. Mya, X. Lu and C. He, *J. Mater. Chem.*, 2009, **19**, 4740.
47 Y. Gao, A. Eguchi, K. Kakehi and Y. C. Lee, *Org. Lett.*, 2004, **6**, 3457.
48 Y. Mai and A. Eisenberg, *Chem. Soc. Rev.*, 2012, **41**, 5969.
49 L. Zhang and A. Eisenberg, *Polym. Adv. Technol.*, 1998, **9**, 677.
50 L. Zhang and A. Eisenberg, *J. Am. Chem. Soc.*, 1996, **118**, 3168.
51 P. Bhargava, Y. Tu, J. X. Zheng, H. Xiong, R. P. Quirk and S. Z. D. Cheng, *J. Am. Chem. Soc.*, 2007, **129**, 1113.
52 P. Bhargava, J. X. Zheng, P. Li, R. P. Quirk, F. W. Harris and S. Z. D. Cheng, *Macromolecules*, 2006, **39**, 4880.
53 A. Goldsipe and D. Blankschtein, *Langmuir*, 2005, **21**, 9850.
54 A. Goldsipe and D. Blankschtein, *Langmuir*, 2006, **22**, 3547.